RSC Advances

ROYAL SOCIETY OF CHEMISTRY

www.rsc.org/advances

Enhanced thermal decomposition and kinetics of Poly (Lactic Acid) sacrificial polymer catalyzed by metal oxide nanoparticles

Lu Liu[a], Michael R. Zachariah*[ab], Stanislav I. Stoliarov[c], Jing Li*[d]

a. Department of Chemistry and Biochemistry, University of Maryland, College Park, MD 20742, USA
b. Department of Chemical and Biomolecule Engineering, University of Maryland, College Park, MD 20742, USA
c. Department of Fire Protection Engineering, University of Maryland, College Park, MD 20742, USA
d. Department of Fire Science & Professional Studies, University of New Haven, West Haven, CT, 06516, USA

ABSTRACT: Poly Lactic Acid (PLA) has been used as sacrificial polymer in the fabrication of battery separators and can be employed in 0D-3D Vaporization of a Sacrificial Component (VaSC) fabrication. In this study, 1wt% PLA/Fe_2O_3, PLA/CuO, PLA/Bi_2O_3 composites are prepared by solvent evaporation casting. Scanning Electron Microscopy (SEM) images indicate that the embedded nanoparticles are well dispersed in the polymer matrix and X-Ray Diffraction (XRD) verifies the crystallinity of these Metal Oxides (MOs). Thermal stability analysis of PLA and PLA/MO composites is performed using a Thermogravimetric Analyzer (TGA) and Differential Scanning Calorimeter (DSC). The overall heat of combustion is measured by Microscale Combustion Calorimetry (MCC) and is found to be insensitive to the presence of nanoparticles. The overall catalytic effects of the three metal oxides trends as: Bi_2O_3>Fe_2O_3>CuO ≈ inert material. PLA/Bi_2O_3 decomposition onset temperature ($T_{5\%}$) and

maximum mass loss decomposition temperature (T_{max}) are lowered by approximately 75 K and 100 K respectively compared to the neat PLA. The as-synthesized Bi_2O_3 is identified as the most effective additive among those proposed in the literature to catalyze the PLA thermal decomposition process. A numerical pyrolysis modeling tool, ThermaKin, is utilized to analyze thermogravimetric data of all the PLA/MOs and to produce a description of the decomposition kinetics, which can be utilized for modeling of thermal vaporization of these sacrificial materials.

1. Introduction

Poly Lactic Acid (PLA) is an environmentally friendly polymer produced from plants (mainly from starch and sugar) including corn, potatoes and sugar-beets, and has attracted attention for its biocompatibility, biodegradability, and thermoplastic processability.[1] It has been reported that the greenhouse gas emission rate of PLA is approximately 1600 kg CO_2/metric ton, while that of polypropylene (PE), polystyrene (PS), polyethylene terephthalate (PET), and nylon are 1850, 2740, 4140, and 7150 kg CO_2/metric ton, respectively.[2] Further, PLA's low temperature of thermal degradation with minimal solid residue (gasified lactide) has made it an attractive candidate as a sacrificial component in polymer fabrication.[2-4]

PLA is also one of the two major plastics explored as 3D printing inks (the other being Acrylonitrile Butadiene Styrene (ABS)) because of its thermoplastic properties.[5] Although ABS is currently the dominant 3D printing polymer, PLA offers the advantage of bio-compatibility. As a sacrificial component, PLA can be 3D printed to create complex-shaped molds[6-8]. For example, White *et al.*[7] have fabricated PLA as spheres (0D), fibers (1D), sheets (2D), and 3D printed sacrificial materials, leaving behind the reverse replica. Pitet *et al.*[9] have explored PLA as a sacrificial component in copolymers to create porous membranes for battery separators utilizing the fact that its decomposition temperature is about 200^{o}C lower than thermally stable polymers such as polyimide (PI), epoxies, Poly(vinylidene fluoride-hexafluoropropylene) (PVDF-HFP), *etc*. The decomposition of neat PLA occurs above ~550K, which can lead to the thermal instability of other polymer blends in practical applications during prolonged heat treatment[7]. Therefore, alkali earth metal oxides[3], rare metal (scandium (III) triflates (CF_3SO_3-))[10], and tin-containing compounds[7, 8, 11] were studied as catalysts for PLA thermal decomposition. Moore *et al.*[6, 7] added Sn-based reactants to lower the decomposition temperature by 90 K to effectively remove

sacrificial PLA at a lower temperature while avoiding thermal damage to the epoxy mold. It was found that the same amount of SnO_x additive works even better than tin (II) octoate to further reduce the total decomposition time at the same temperature.[7] Mori *et al.* reported similar results using Sn-based compounds and recognized that these catalysts could enhance the breakage of ester bonds in the polymer backbone, thus promoting the fragmented polymer ends to experience chain backbiting and transesterification reactions before further depolymerization.[11] Almost all of the previous studies used a high loading of more than 5 wt% catalyst.[3, 6-11]

Addition of catalysts into PLA is usually achieved by surface treatment (including impregnation or solvent swelling)[6], solvent evaporation casting[7], or vane extruding.[12] Dong *et al.*[6] utilized solvent swelling to immobilize metal ions (tin (II) octoate solution) into PLA fibers. Later, Moore *et al.* used solvent evaporation to imbed SnO_x into PLA, further decreasing the decomposition temperature.[7] Solvent evaporation casting of PLA with specific viscosity was utilized by Guo *et al*. in a proposed 3D printing ink drying technique.[13, 14] Zhang *et al.* utilized melt blending with a vane extruder with heating to get mono-dispersed PLA/TiO_2 nanocomposites.[12]

It is widely known that controlling the removal process of the sacrificial materials is extremely difficult, requiring carefully designed thermal conditions and perfect timing to fully eliminate the sacrificial material at minimal cost, while also keeping the host material undamaged.[15, 16] Therefore, catalysts are added to increase the decomposition temperature difference between the sacrificial materials and host materials to maintain the integrity of the host polymer.[3, 6-11] Usually the removal time for even nano-scale channels are hours to days and are highly non-linear relative to different heating conditions, which makes the control process hard to predict.[6, 7, 15] The severity of this problem increases as larger and more complex

74 geometries are required with the rapid development of 3D printing using such sacrificial
75 materials.[13, 14] MOs have not been studied extensively as catalysts for PLA, especially at small
76 loadings (< 5%)[3,6,11].

77 In this work, we employed 1 wt% MOs loading to study the catalytic effects of MOs. Bi_2O_3,
78 CuO and Fe_2O_3 are synthesized by spray pyrolysis[17-19] and then uniformly embedded into PLA
79 matrix using solvent evaporation casting. XRD and SEM are performed to verify the additives'
80 crystallinity and homogenous dispersion in the PLA matrix. The thermal properties of
81 PLA/MOs composites relative to neat PLA are measured by TGA (Thermogravimetric Analyzer),
82 DSC (Differential Scanning Calorimeter), and MCC (Microscale Combustion Calorimeter) to
83 examine the MOs catalytic effect on the PLA's thermal degradation process and overall
84 combustion heat. Thermal degradation simulations are performed to fit the experimental TGA
85 curve with a number of first order chemical pyrolysis reaction models using a one dimensional
86 pyrolysis model (-ThermaKin[20] running under thermally thin mode). This kinetic fitting work is
87 preformed to reproduce the TGA data, which provides kinetic fundamentals to potentially further
88 predict and control the removing process time and temperatures of PLA/MOs for different
89 geometries or length scales in various heating environments in the future.

90 **2. Experimental**

91 All metal oxide additives are in-house synthesized by aerosol spray pyrolysis.[17-19] The spray
92 pyrolysis system (pictured in Figure 1) consists of an atomizer (to produce aerosol droplets), a
93 silica-gel diffusion drier (to remove solvent), an isothermal furnace (to decompose precursor
94 droplets), and a stainless steel sample collector with 0.4 μm DTTP Millipore filter (to collect
95 nanoparticles). The aerosol droplets of precursor solution are generated using a collision-type
96 nebulizer with an initial droplet diameter of approximately 1μm, which is then desiccated by

passing through the silica-gel diffusion dryer. The dehydrated aerosol precursors then decompose into the solid metal oxide particles in the tube furnace set at 600 ^{o}C for Fe_2O_3 and CuO, or 1050^{o}C for Bi_2O_3, with a residence time of about 1s. Particles exiting the aerosol reactor are then collected on a 0.4 μm pore size DTTP Millipore filter with 10%-20% porosity (EMD Millipore). The precursors used for the Bi_2O_3, Fe_2O_3, and CuO are $Bi(NO_3)_3{\cdot}5H_2O$, $Fe(NO_3)_3{\cdot}9H_2O$ and $Cu(NO_3)_2{\cdot}3H_2O$ respectively, all from Sigma-Aldrich. A total precursor concentration of 0.200 M aqueous solution is used for MOs, and to dissolve $Bi(NO_3)_3{\cdot}5H_2O$, 1:5 concentrated nitric acid and water mixture is used as the solvent. The aerosol spray pyrolysis is a droplet to droplet method, and the formation mechanism of MOs is described in Figure 1 below. Lognormal poly-dispersed spherical solid particles are generated e.g. the Fe_2O_3 particles are spherical particles with a lognormal distribution peak at 84nm.[19]

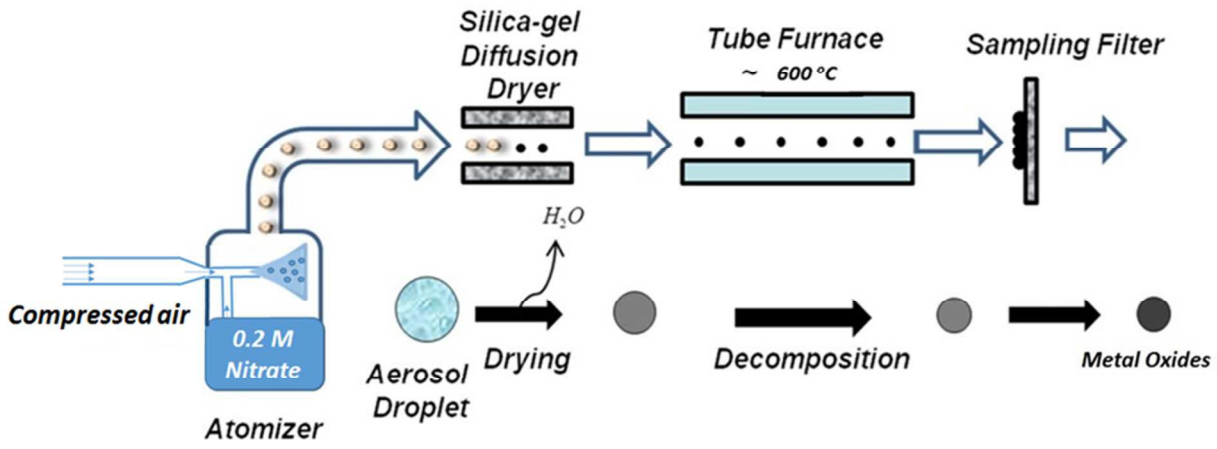

Figure 1. Aerosol spray pyrolysis synthesis system for metal oxides.

PLA (Rejuven8 Plus Spartech) is obtained from Nature Works and used as received. The PLA sheets are 0.7 mm thick and cut into small pieces for solvent evaporation casting. 1.000 g PLA is first dissolved in 100.0 mL CH_2Cl_2 with magnetic stirring for 30 mins. Then 10.0 mg (1wt%) MO is added to the solution and ultra-sonicated for 1h. The solutions are then poured

onto a watch glass and dried in a 50 ^{o}C convection oven to for 12h. Thin films of neat PLA (baseline reference) and PLA/MO composites are obtained after solvent evaporation. Small pieces of the as prepared thin films were then used for the thermal tests. Crystal structures of metal oxides are characterized by XRD with a Bruker Smart1000 using Cu Kα radiation. SEM results were obtained by Hitachi SU-70 SEM. For cross-sectional SEM images, samples are first fractured in liquid nitrogen and then sputter-coated with carbon. Nitrogen (N_2) adsorption-desorption isotherms and Brunauer–Emmett–Teller (BET) surface were measured at 77 K with an Micromeritics ASAP 2020 Porosimeter.

A Netzsch F3 Jupiter Simultaneous Thermal Analyzer (STA), employed in the thermal stability study, combines a TGA equipped with a 1 μg-resolution microbalance and DSC heat flow measurement with a steel furnace. Thus the STA can measure the TGA and DSC signals simultaneously during a single experiment. The PLA/MOs films were stored in a desiccator for 48 hours prior to testing, and then cut and pressed into Platinum-Rhodium crucibles with ventilation lids with a sample mass of 6-7 mg. The thermal decomposition experiments were performed at a heating rate of 10 K min^{-1} from 40 ^{o}C to 600 ^{o}C under 99.999% (UHP) N_2 at a flow rate of 50 cm^3·min^{-1}. A microscale combustion calorimeter (MCC) with 3 mg samples was used to measure the heat release rate and total heat of combustion.[1] The MCC combines a condensed phase pyrolyzer and gas phase combustor. The samples are first decomposed in 80 cm^3 min^{-1} UHP N_2 flow, 60 K min^{-1} heating rate from 75 to 600 ^{o}C inside the pyrolyzer, which is similar to the STA furnace, and then transferred to the combustor where the gaseous fuel (decomposition products) was burned at 950 ^{o}C to ensure complete combustion mixing with additional 20 cm^3·min^{-1} O_2. The entire experimental measurement of HRR (Heat Release Rate) followed ASTM standard ASTM D 7309-13.[21] The heat release rate is measured based on

Thornton's rule by measuring the O_2 consumption rate of combustion.[22]

3. Results and Discussion

Figure 2 shows the SEM micrographs of spray pyrolysis synthesized Bi_2O_3, Fe_2O_3 and CuO nanoparticles, which are solid spherical particles with diameters from 50nm to 1μm following a log normal distribution with a peak (Fe_2O_3 at 84 nm[19], CuO at 86nm and Bi_2O_3 at 87 nm, shown in Figure S1). Figure S2 shows BET surface area results: Fe_2O_3-13 m^2/g, CuO-23 m^2/g, Bi_2O_3-4 m^2/g, with Bi_2O_3 surface area being the lowest, indicating that surface area does not explain the superior catalytic activity of Bi_2O_3. The crystal structure of oxides are investigated from XRD shown in Figure S3. All peaks in Fe_2O_3 can be indexed to γ-Fe_2O_3 phase (JCPDS card No.: 39-1346); Bi_2O_3 with JCPDS card No.: 27-0050, while CuO peaks corresponds to tenorite with JCPDS card No.: 48-1548.

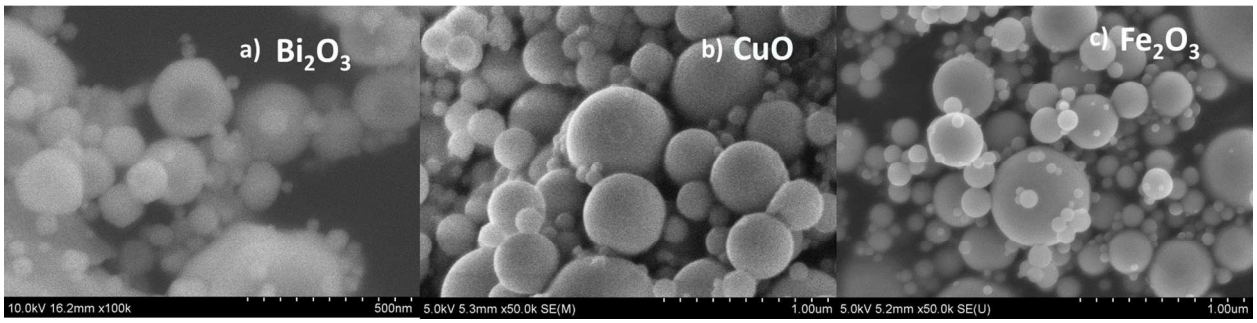

Figure 2. SEM of nanoparticles a) Bi_2O_3, b) CuO, c) Fe_2O_3, prepared from spray pyrolysis.

It is widely known that the dispersion of nanoparticles in polymer will greatly influence the both chemical and physical properties of the PLA/MO composites. Homogeneous dispersion of MO nanoparticles will affect the thermal and mechanical behaviors of PLA, such as wettability, UV transmittance, strength and ductility, elasticity, viscosity, antibacterial property.[12]

Cross-sectional SEM images are taken to check the dispersion of MOs in the composites. PLA/MOs are first fractured in liquid nitrogen and then broken off for cross-sectional images. Figure 3a) and 3b) show neat PLA cross-sectional image without particles, and Figure 3c) and 3d) are PLA/Fe_2O_3, PLA/CuO films images, respectively. It is clear from these images that all nanoparticles are well dispersed in the PLA films. Figure 4 shows the cross-sectional PLA/Bi_2O_3 structure, and it is clear that spherical Bi_2O_3 are uniformly dispersed in PLA and un-aggregated. The film is about 50 μm thick, indicated by low magnification image of Figure 4a) and Figure 4b). Moreover, Figure 4c) and 4d) give a closer view of the cross-sections, all showing that particles are coated and/or connected by PLA while separated from other nanoparticles.

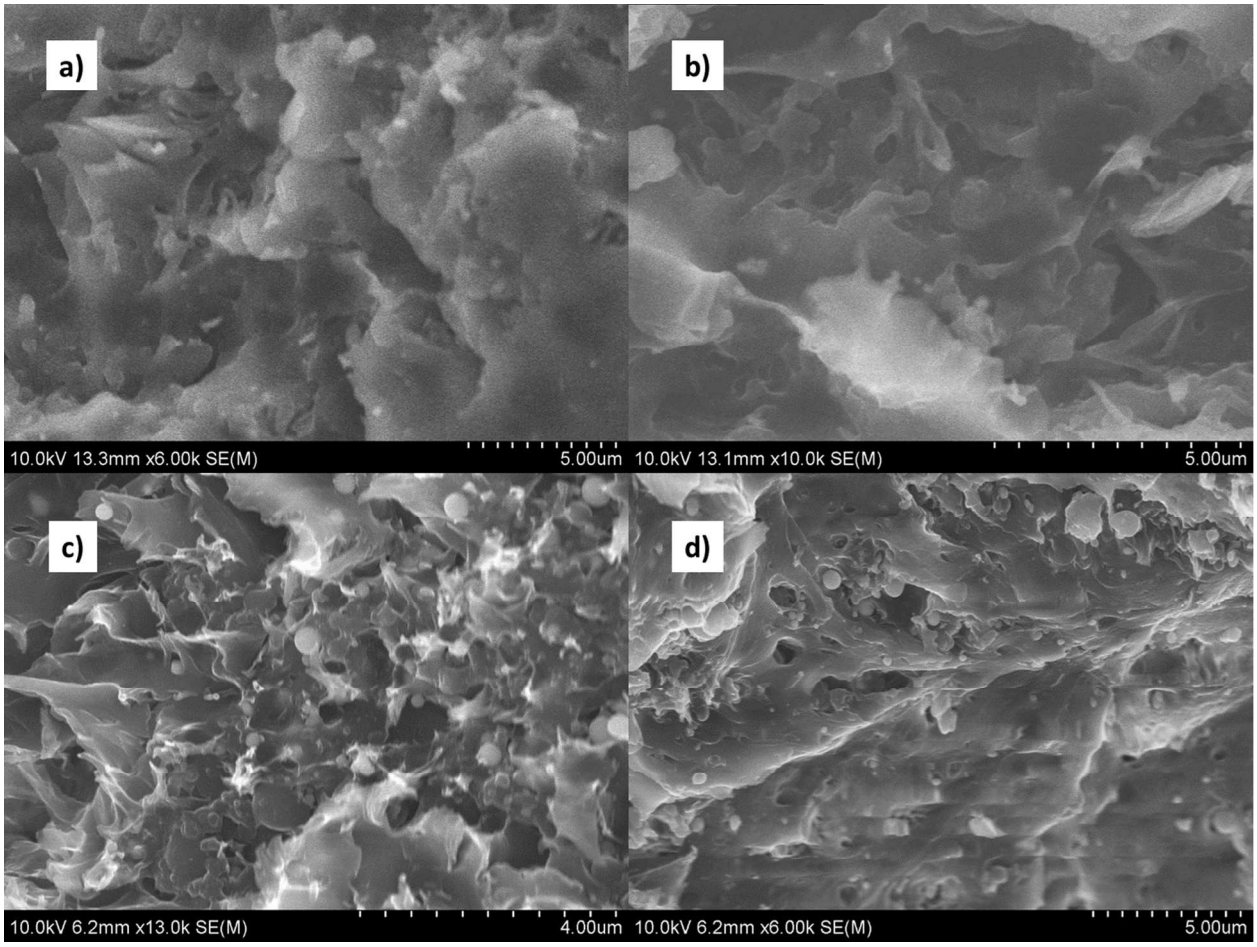

Figure 3. SEM of cross-sectioned a) and b) PLA, c) PLA/Fe_2O_3, d) PLA/CuO films.

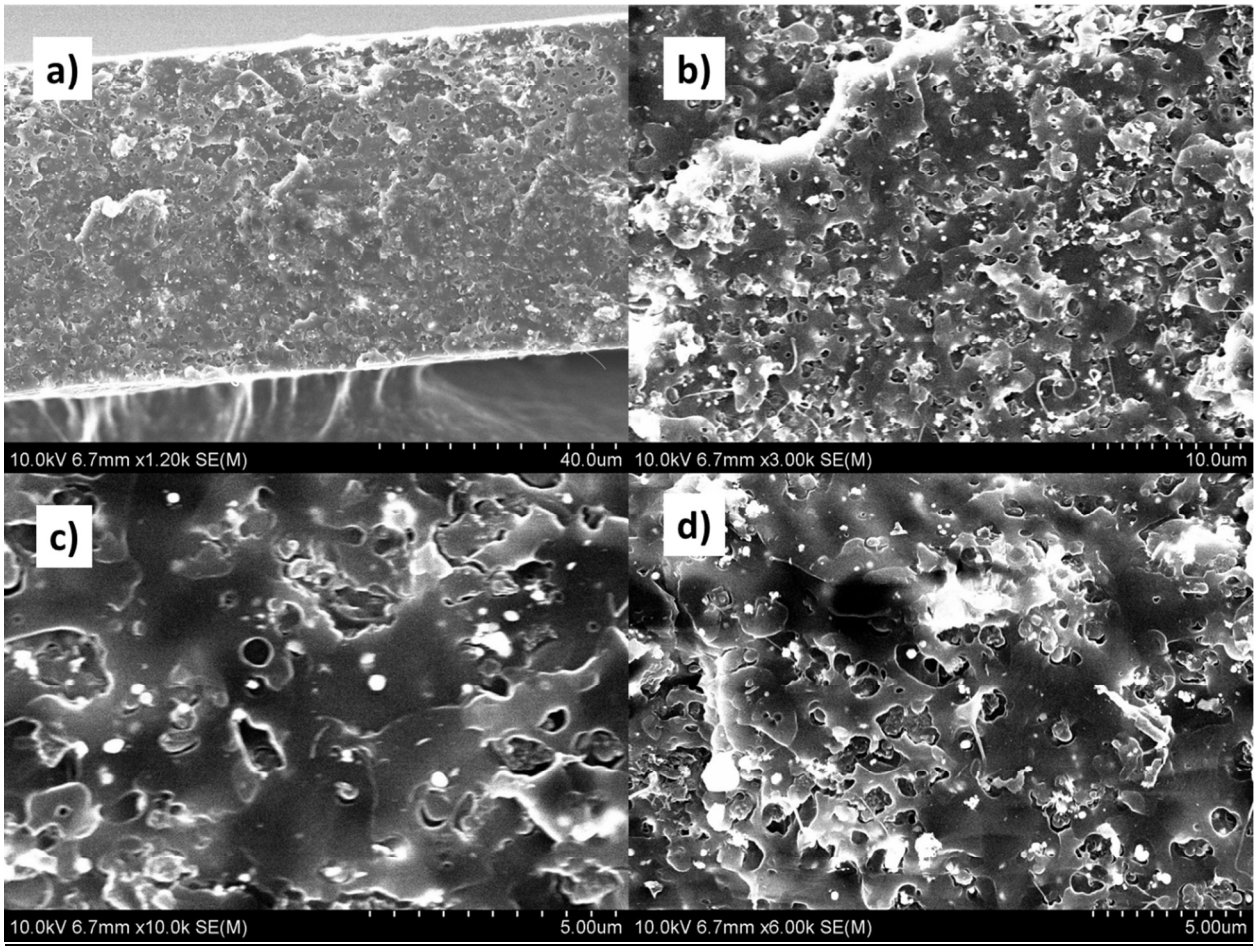

Figure 4. SEM of cross-sectioned PLA/Bi_2O_3 film.

Figure 5 shows the TGA data of thermal decomposition mass loss under N_2 inert atmosphere. It is clear that the various types of MO additives affect the thermal stabilities of PLA/MOs differently, which can also be clearly seen in Figure 6 from Derivative Thermogravimetry (DTG) experimental curves (dotted lines). Specifically, the onset thermal degradation temperature for neat PLA as a reference is approximately $T_{5\%} \approx 580$ K. For PLA/Bi_2O_3, this temperature is 75 K lower ($T_{5\%} \approx 505$ K), while the effect of Fe_2O_3 is about 30 K decrease ($T_{5\%} \approx 550$ K) compared to neat PLA; CuO shows no noticeable effect. The thermal degradation temperatures at maximum weight loss (T_{max}), are 536 K (614 K for the second peak),

573 K, 634 K and 635 K for PLA/Bi_2O_3, PLA/ Fe_2O_3, PLA/CuO and neat PLA respectively. These results show that the catalytic properties trend as: Bi_2O_3>Fe_2O_3>CuO. While the DSC signals reveal notable differences at the stage of decomposition, the addition of MOs does not significantly affect the melting point ~ 425 K or the heat of melting (as seen in DSC Figure 7). The heats of melting (the first peak integrals) are within 4% difference of their mean.

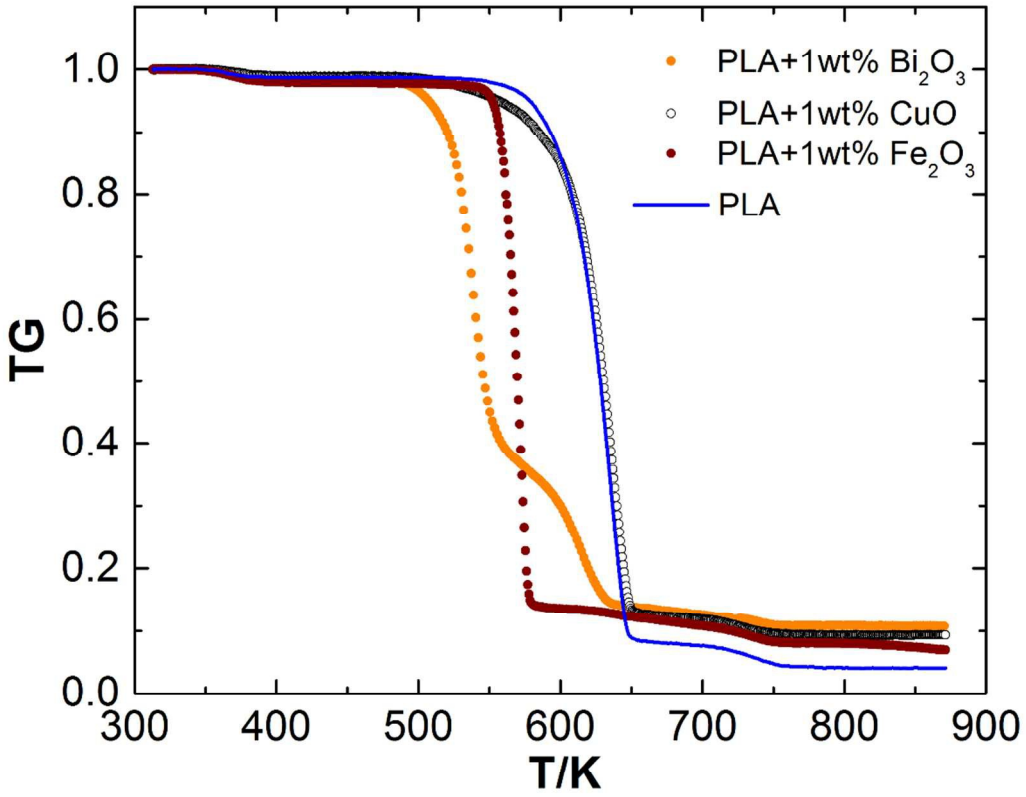

Figure 5. TGA of PLA and PLA/MOs.

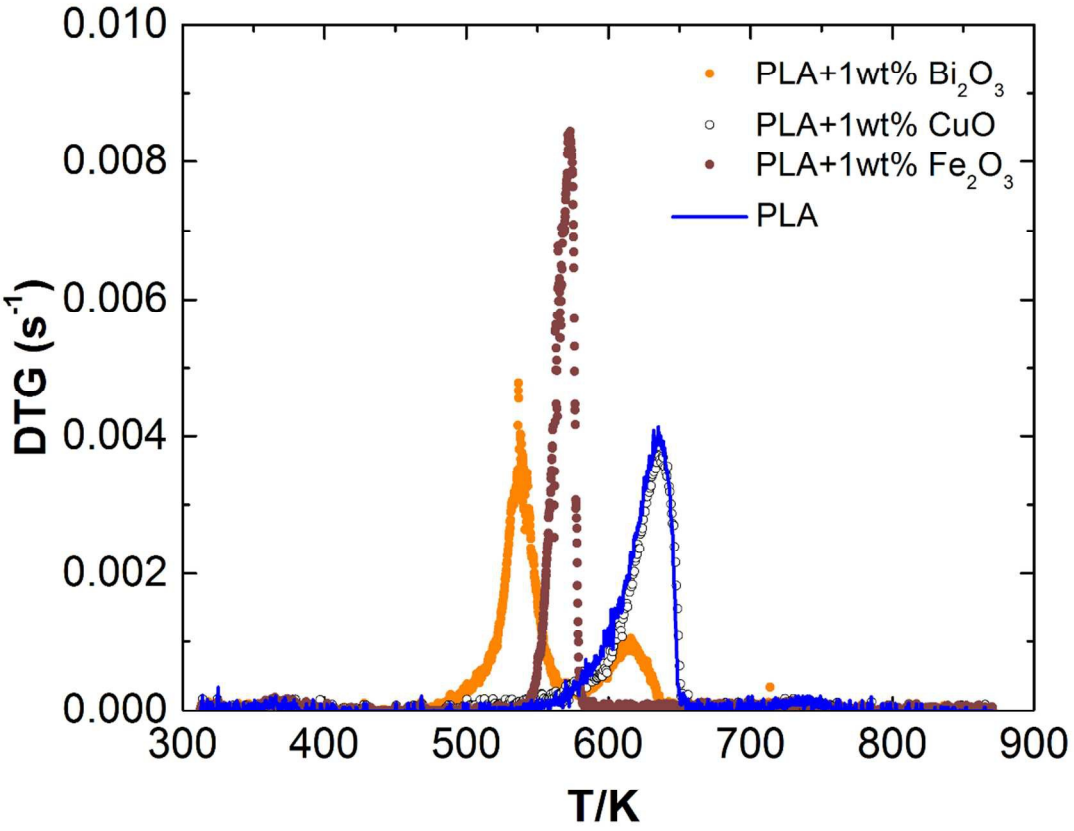

Figure 6. DTG plots of PLA and PLA/MOs.

To better evaluate the decomposition kinetics at various heating conditions and scales, which are necessary as fundamentals to predict the catalytic effects of the MOs on the PLA decomposition, we have extracted phenomenological rate parameters using a numerical pyrolysis software - ThermaKin.[20] ThermaKin solves the mass and energy conservation equations numerically for one or two dimensional objects exposed to external (convective and/or radiative) heat. In this study, we use the thermally thin mode to simulate the thermal degradation processes inside the STA furnace. The material of the object (sample) is described by multiple components, which may interact chemically and physically. The neat PLA and PLA/MOs kinetics were

characterized using the methodology reported in our recent publications.[23] This methodology has been successfully applied to reproduce TGA and DSC signals of 15 non-charring and charring polymers.[23,24] The resulting kinetic parameters were also shown to predict gasification or burning rates of these polymers at a wide range of thermal conditions.[23-26]

In the previous study, neat PLA was tested using STA and the kinetics of its decomposition was modeled using two consecutive first order reactions.[23] One more reaction was employed to describe melting (T_{melt} = 425 K). This was done to use a minimum number of parameters to describe the entire time-resolved TGA and DSC curves. The kinetics of those reactions are parameterized with Arrhenius parameters (A_x, E_x represent decomposition reaction x; while A_m, E_m represent the melting) listed in Table 1. The value of the θ_x is calculated by the instantaneous mass (at the end stage of the reaction x) over its initial mass. Note that the θ_x, obtained directly from the TGA experiments, corresponds to the remaining condensed phase residue yielded in the reaction x. Those parameters are initially estimated using simple analytical expressions[27] and then changed in small increments following the rules summarized in the previous studies until agreements with the experiment is reached (based on preset coefficient of determination and visual comparison). Each model reaction corresponds to tens or, perhaps, hundreds of elementary chemical processes operating within the same range of temperatures.

The MOs do not affect the phase transition as evident from DSC curves in Figure 7 (enlarged temperature range in the left corner). The kinetic parameters describing the melting were reported previously[23]. For all the PLA composites, MOs are found to affect the thermal degradation process significantly, which is apparent in both the TGA and DSC measurements. The impact of MOs on the kinetics of decomposition is quantified through changes in the parameters of the first (major) reaction. The kinetic parameters are summarized in Table 1. With

218 the exception of PLA/Bi_2O_3, the decomposition of all composites can be described by two
219 consecutive reactions. The kinetics of the second reaction remain unaffected by the addition of
220 MOs. In the case of PLA/Bi_2O_3, the thermal decomposition process consists of three consecutive
221 reactions reflecting a more complex DTG signal. It has been widely concluded that the thermal
222 decomposition of pure PLA is a one-stage reaction that involves the loss of ester groups in pure
223 nitrogen[28] and air[29, 30], consistent with our observations for neat PLA and PLA/CuO in this study.
224 Other researchers have also observed multiple reaction steps with the addition of other catalysts[6],
225 although little information on mechanism is available. Our speculation for the existing second
226 peak is that part of the PLA remains unaffected by the catalytic Bi_2O_3 during the first
227 decomposition step, and it decomposes as neat PLA at a higher temperature to form the second
228 peak. Further investigation is required to validate this hypothesis.

229 For all the materials, the solid lines in Figure 8 represent the numerical simulation results
230 from the ThermaKin. All the simulation results fit the experimental data well and the calculated
231 coefficients of determination of the experimental data and the fitted curves are all above 0.9.

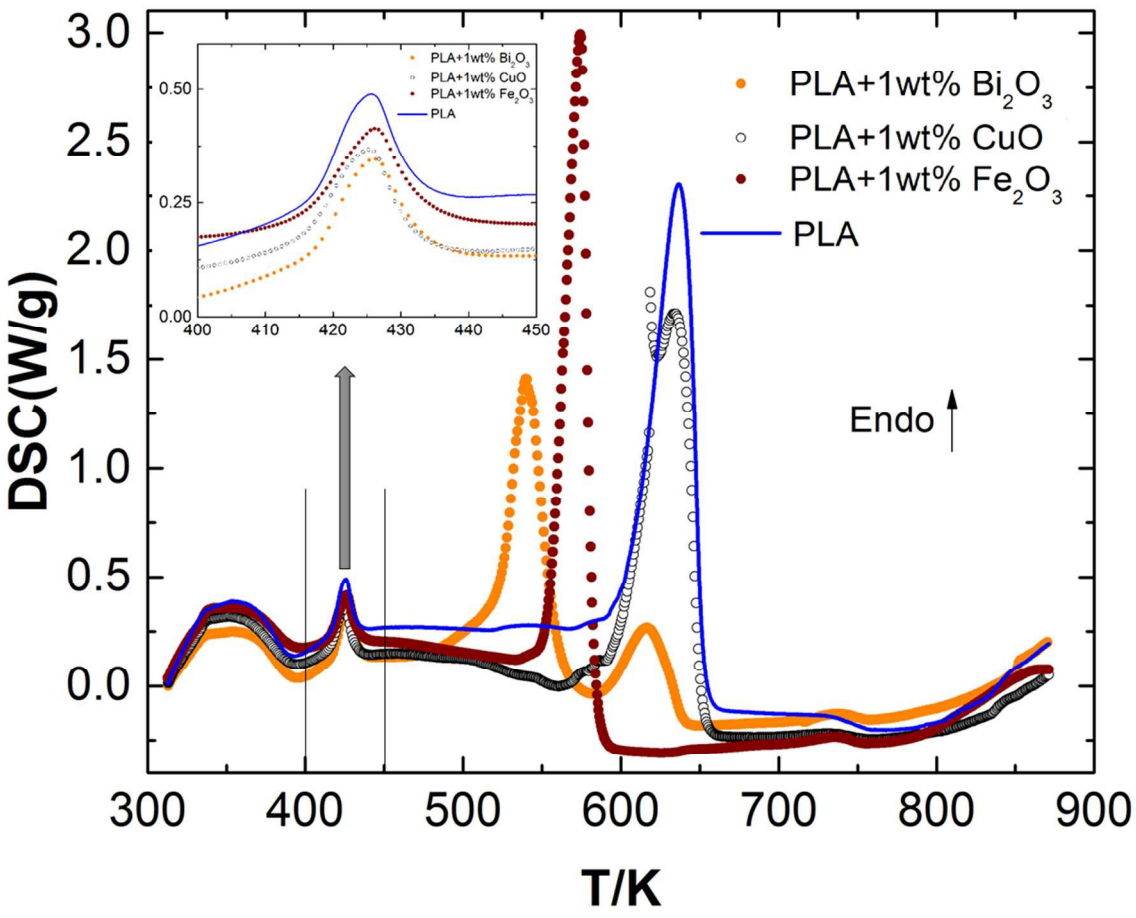

232

233 **Figure 7.** DSC test of PLA and PLA/MOs.

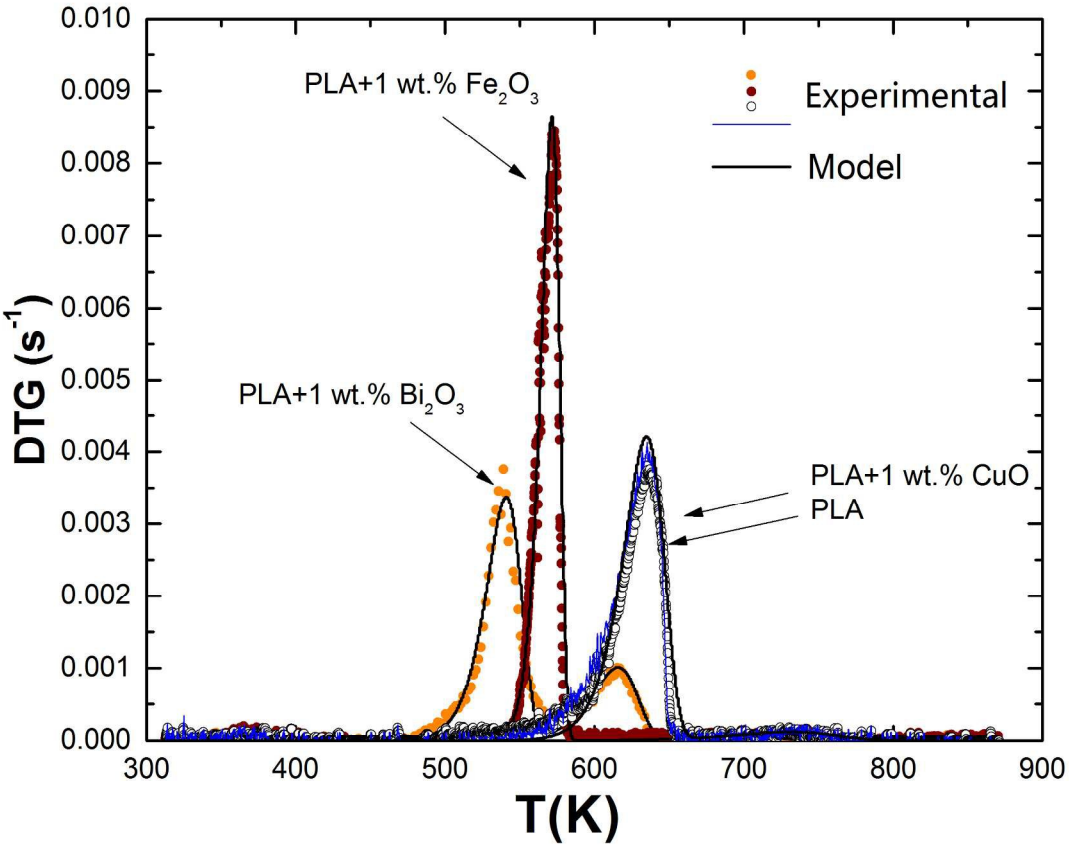

234

235 **Figure 8.** Experimental and simulated DTG of PLA & PLA/MO composites at 10 K min^{-1}.

236

Polymer	A_1 (s^{-1})	E_1 (kJ mol^{-1})	θ_1	A_2 (s^{-1})	E_2 (kJ mol^{-1})	θ_2	A_3 (s^{-1})	E_3 (kJ mol^{-1})	θ_3	A_m (s^{-1})	E_m (kJ mol^{-1})
PLA	1.68E18	245	0.1	4.58E6	126	0.4	N/A	N/A	N/A	6.0E40	355
PLA+ Fe_2O_3	1.80E38	436	0.14	4.58E6	126	0.5	N/A	N/A	N/A	6.0E40	355
PLA+	1.34E18	207	0.38	2.85E15	205.5	0.37	4.58E6	126	0.72	6.0E40	355

Bi_2O_3											
PLA+ CuO	1.68E18	245	0.1	4.58E6	126	0.4	N/A	N/A	N/A	6.0E40	355

237 Table 1 Kinetic parameters for PLA, PLA/Fe_2O_3, PLA/Bi_2O_3 and PLA/CuO.

238 The Heat Release Rate(HRR) is measured by MCC, as shown in the Figure 9. The heat
239 release rate curves for all the PLA/MOs composites match the reaction peaks of TGA and DSC
240 qualitatively but not quantitatively with respect to their peak temperatures. The corresponding
241 heat release rate peaks in Figure 9 for all the samples shift to a higher temperature by
242 approximately 27 ~ 28 K compared to the DTG and DSC results in Figures 6 & 7.

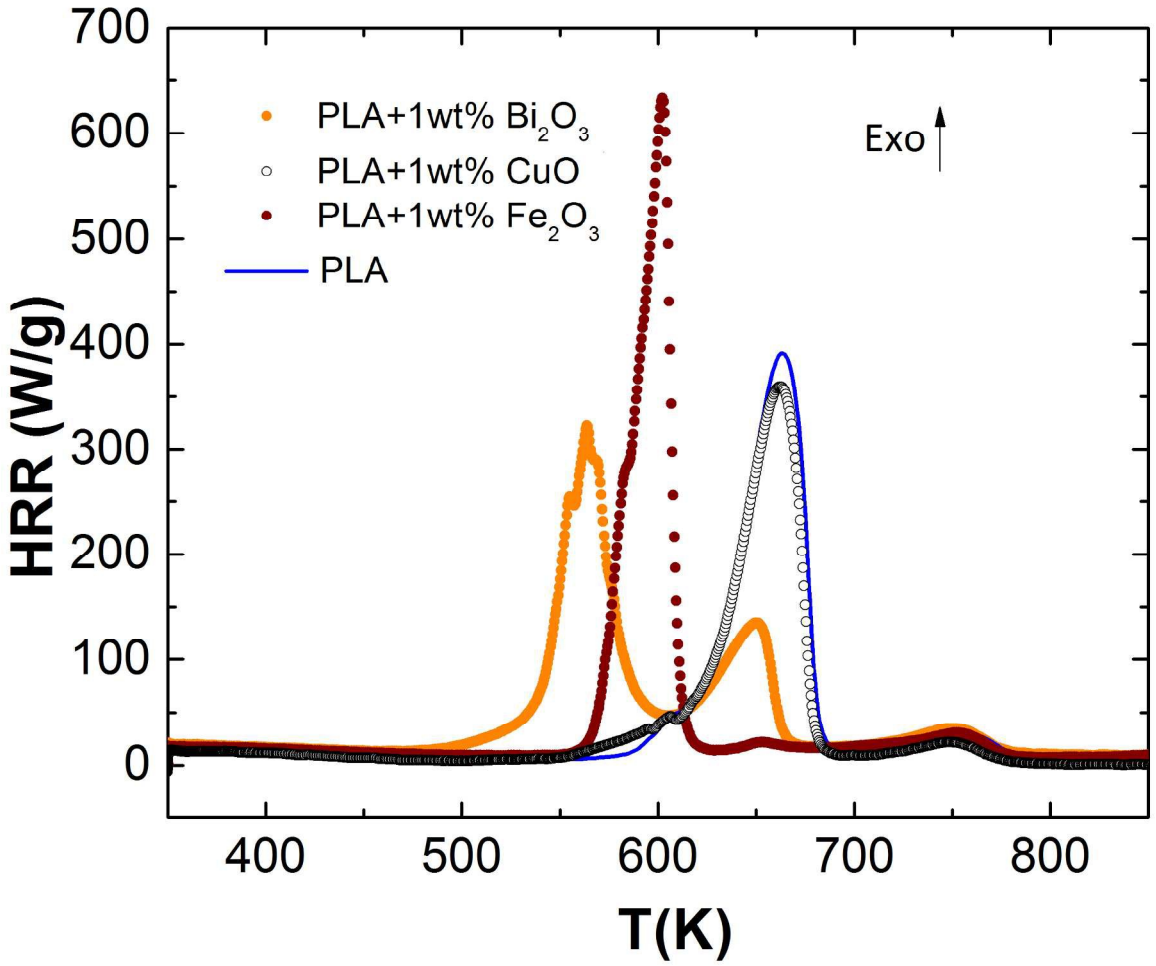

Figure 9 HRR of PLA, PLA/Fe_2O_3, PLA/Bi_2O_3 and PLA/CuO.

This temperature difference is caused by the relatively higher heating rate (60 K min^{-1}) utilized in the MCC compared to the heating rate (10 K min^{-1}) in the STA test. The integral of the heat release rate, which accounts for the heat of combustion of the gaseous decomposition products, is approximately equal for all tested samples yielding 19.5±0.8 kJ/g. Therefore, all of the these three types of 1wt% PLA/MOs affect the thermal degradation processes only in the condensed phase but have no effect on the heat of combustion.

4. Conclusion

In this paper, we offer a facile method to incorporate metal oxide additives and evaluate their catalytic effects on PLA thermal decomposition. More specifically, we have explored Bi_2O_3, CuO and Fe_2O_3 nanoparticles as catalysts for PLA thermal decomposition. Bi_2O_3 is shown to be a highly effective catalyst for PLA thermal decomposition. With only 1wt% loading, it lowered the onset decomposition temperature ($T_{5\%}$) by 75 K and the decomposition temperature at the maximum weight loss (T_{max}) by approximate 100 K, comparable to the most effective catalysts studied so far. The same amount of Fe_2O_3 and CuO nanoparticles have moderate and negligible effects on PLA thermal decomposition processes respectively. The overall catalytic effects of the three metal oxides trend as: $Bi_2O_3 > Fe_2O_3 > CuO \approx$ inert material.

The complete heats of combustion for the PLA/MOs composites have been measured by MCC, in which 1wt% MO additive catalyzes the thermal degradation processes differently in the condensed phase, and moreover, have negligible effect on the complete combustion heat in the gas phase as expected. PLA/MOs decomposition was then quantatatively analysed to extract Arrhenious parameters for the decomposition kinetics, which offers possible explanations and predictions to evaluate thermal decompostion kinetics at other heating rate conditions.

5. Acknowledgement

This work was partially supported by faculty research fund from the University of New Haven. The authors would like to thank Ms. Xi Ding for conducting the MCC tests.

6. Reference

1. R. E. Drumright, P. R. Gruber and D. E. Henton, *Advanced Materials*, 2000, **12**, 1841-1846.
2. Y. Fan, H. Nishida, Y. Shirai, Y. Tokiwa and T. Endo, *Polymer Degradation and Stability*, 2004, **86**, 197-208.

3. Y. Fan, H. Nishida, T. Mori, Y. Shirai and T. Endo, *Polymer*, 2004, **45**, 1197-1205.
4. C. Gottschalk and H. Frey, *Macromolecules*, 2006, **39**, 1719-1723.
5. M. Kreiger and J. M. Pearce, *ACS Sustainable Chemistry & Engineering*, 2013, **1**, 1511-1519.
6. H. Dong, A. P. Esser-Kahn, P. R. Thakre, J. F. Patrick, N. R. Sottos, S. R. White and J. S. Moore, *ACS Applied Materials & Interfaces*, 2012, **4**, 503-509.
7. R. C. R. Gergely, S. J. Pety, B. P. Krull, J. F. Patrick, T. Q. Doan, A. M. Coppola, P. R. Thakre, N. R. Sottos, J. S. Moore and S. R. White, *Advanced Functional Materials*, 2015, **25**, 1043-1052.
8. F. Carrasco, P. Pagès, J. Gámez-Pérez, O. O. Santana and M. L. Maspoch, *Polymer Degradation and Stability*, 2010, **95**, 116-125.
9. L. M. Pitet, M. A. Amendt and M. A. Hillmyer, *J Am Chem Soc*, 2010, **132**, 8230-8231.
10. T. S. Coope, U. F. J. Mayer, D. F. Wass, R. S. Trask and I. P. Bond, *Advanced Functional Materials*, 2011, **21**, 4624-4631.
11. T. Mori, H. Nishida, Y. Shirai and T. Endo, *Polymer Degradation and Stability*, 2004, **84**, 243-251.
12. H. Zhang, J. Huang, L. Yang, R. Chen, W. Zou, X. Lin and J. Qu, *RSC Advances*, 2015, **5**, 4639-4647.
13. S.-Z. Guo, F. Gosselin, N. Guerin, A.-M. Lanouette, M.-C. Heuzey and D. Therriault, *Small*, 2013, **9**, 4118-4122.
14. S.-z. Guo, X. Yang, M.-C. Heuzey and D. Therriault, *Nanoscale*, 2015, **7**, 6451-6456.
15. H. A. Reed, C. E. White, V. Rao, S. Ann, B. Allen, C. L. Henderson and P. A. Kohl, *J. Micromech. Microeng.*, 2001, **11**, 733-737.
16. S. Metz, S. Jiguet, A. Bertsch and P. Renaud, *Lab on a Chip*, 2004, **4**, 114-120.
17. C. Wu, K. Sullivan, S. Chowdhury, G. Jian, L. Zhou and M. R. Zachariah, *Advanced Functional Materials*, 2012, **22**, 78-85.
18. G. Jian, L. Liu and M. R. Zachariah, *Advanced Functional Materials*, 2013, **23**, 1341-1346.
19. L. Liu and M. R. Zachariah, *Energy & Fuels*, 2013, **27**, 4977-4983.
20. S. I. Stoliarov and R. E. Lyon, *Thermo-Kinetic Model of Burning*, Federal Aviation Administration Technical Note, 2008.
21. ASTM(D7309-13), *Standard Test Method for Determining Flammability Characteristics of Plastics and Other Solid Materials Using Microscale Combustion Calorimetry* 7309, 2013.
22. W. Thornton, *Philosophical Magazine and J. of Science*, 1917, **33**, 196-203.
23. J. Li and S. I. Stoliarov, *Combust Flame*, 2013, **160**, 1287-1297.
24. J. Li, J. Gong and S. I. Stoliarov, *Int J Heat Mass Tran*, 2014, **77**, 738-744.
25. J. Li and S. I. Stoliarov, *Polymer Degradation and Stability*, 2014, **106**, 2-15.
26. J. Li, J. Gong and S. I. Stoliarov, *Polymer Degradation and Stability*, 2015, **115**, 138-152.
27. R. E. Lyon, R. N.Walters and S. I. Stoliarov, *Journal of ASTM International*, 2006, **3**, 1-18.
28. M. A. G. Cristian-Andi Nicolae, Raluca Augusta Gabor, *Engineering Letter*, 2008, **16**.
29. M. C. G. a. V. G. Deshmukh, *Coll Polym. Sci.,*, 1982, **260**, 514-517.
30. M. C. G. a. V. G. Deshmukh, *Coll. Polym. Sci*, 1982, **260**, 308-311.